POST BEAMFORMING ADAPTIVE SECOND ORDER VOLTERRA FILTER (ASOVF) FOR PULSE-ECHO ULTRASONIC IMAGING

Mamoun Fawzi Al-Mistarihi
e-mail: mistarihi@just.edu.jo
Jordan University of Science and Technology, Faculty of Engineering, Department of Electrical Engineering, Irbid 22110, Jordan

Key words: Beamforming, Ultrasound Contrast Agents, Volterra Filter

ABSTRACT

We have previously introduced post-beamforming second order Volterra filter (SOVF) for decomposing the pulse echo ultrasonic radio-frequency (RF) signal into its linear and quadratic components. Using singular value decomposition (SVD), an optimal minimum-norm least squares algorithm for deriving the coefficients of the linear and quadratic kernels of the SOVF was developed and verified. However, the agent specificity of the standard SVD-based quadratic kernel is sometimes compromised by sensitivity to nonlinear echoes from tissue. In this paper, we present an adaptive second-order Volterra filter (ASOVF) designed to obtain the optimum filter coefficients minimizing the cost function to produce images with high sensitivity to nonlinear oscillations (20 - 30 dB below the fundamental) from microbubble ultrasound contrast agents (UCA) while maintaining high levels of noise rejection. The least-squares approach of a second-order Volterra model and its adaptive filtering algorithm based on recursive least-squares are introduced.

I. INTRODUCTION

Microbubble ultrasound contrast agents (UCA) are being investigated for use in clinical imaging applications for tissue function and for targeted therapeutic applications. The objective is to detect minute concentrations of UCA in the microvasculature during ultrasonic exams thus providing a view of the perfusion in the tissue. This functional form of ultrasonic imaging is seen an important component for the continued use of ultrasound as a medical imaging modality. For example, many tumors without distinguishing characteristics on conventional ultrasound have characteristic blood perfusion patterns that allow for easy detection if a perfusion sensitive imaging is available.

Interaction between microbubbles UCAs and acoustic wave result in nonlinear harmonic echo generation. This phenomenon can be exploited to enhance the echoes from the microbubbles and, therefore, reject fundamental components resulting largely from tissue. Imaging techniques based on nonlinear oscillations have been designed for separating and enhancing nonlinear UCA echoes from a specified region of interest within the imaging field, including second harmonic (SH) imaging and pulse inversion (PI) Doppler imaging [2]. The SH imaging employs a fundamental frequency transmit pulse and produces images from the second harmonic component of received echoes by using a second harmonic bandpass filter (BPF) to remove the fundamental frequency. In order to increase UCA detection sensitivity in the limited transducer bandwidth condition, spectral overlap between fundamental and second harmonic parts need to be minimized by transmitting narrow-band pulses resulting in an inherent tradeoff between contrast and spatial resolution. In PI imaging a sequence of two inverted acoustic pulses with appropriate delay is transmitted into tissue. Images are produced by summing the corresponding two backscattered signals. In the absence of tissue motion, the resulting sum can be shown to contain only even harmonics of the nonlinear echoes. The PI imaging overcomes the tradeoff between contrast and spatial resolution because it utilizes the entire bandwidth of the backscattered signals. As a result, superior spatial resolution can be achieved when compared with SH imaging. However, the subtraction process results in significant reduction of signal to noise as the harmonics are typically 20 - 30 dB or more below the (cancelled) fundamental component.

The SOVF-based quadratic kernels provide high sensitivity to harmonic echoes comparable to PI with a significant increase in dynamic range due to inherent noise rejection of quadratic filtering [3]. An algorithm for deriving the coefficients of the kernel using singular values decomposition (SVD) of a linear and quadratic prediction data matrix was proposed and experimentally validated in [4]. Imaging results and comparisons with SH and PI images have shown that quadratic imaging is

superior to SH and compares favorably with PI without the need for multiple transmissions. However, due to reliance on linear and quadratic prediction, the quadratic kernel has sensitivity to the fundamental that limits its ability to detect UCA in the microvasculature.

In this paper, we present an adaptive second-order Volterra filter (ASOVF) designed to obtain the optimum filter coefficients minimizing the cost function to produce images with high sensitivity to nonlinear oscillations (20 – 30 dB below the fundamental) from microbubble ultrasound contrast agents (UCA) while maintaining high levels of noise rejection. The least-squares approach of a second-order Volterra model and its adaptive filtering algorithm based on recursive least-squares are introduced.

The approach is demonstrated experimentally using images from in vivo kidney after bolus injection with UCA. Illustrative images of the kidney of a juvenile pig were obtained before and after infusion of contrast agent (SonoVue, Bracco, Geneva, Switzerland) at various concentrations. Imaging results of ASOVF data show a significant increase in harmonic sensitivity and reduction in noise levels. The imaging results given in this paper indicate that a signal processing approach to this clinical challenge is feasible.

II. THEORY

In this section, we present the basis of an adaptive second-order Volterra filter (ASOVF) designed to. However, for the sake of continuity, we summarize the minimum-norm least-squares (MNLS) approach here (for full detail, please see [3-4]).

A. MNLS Estimation of SOVF Coefficient

The algorithm in this section is based on [3-4], which have shown the validity of a SOVF as a model for pulse-echo ultrasound data from tissue mimicking media. The response of a quadratically nonlinear system with memory $\hat{y}(n+1)$, can be predicted by a second order Volterra model of *m* past values as follows:

$$\hat{y}(n+1) = \sum_{i=0}^{m-1} y(n-i)h_L(i) + \sum_{j=0}^{m-1}\sum_{k=j}^{m-1} y(n-j)y(n-k)h_Q(j,k) \quad (1)$$

where $h_L(i)$ and $h_Q(j,k)$ are the linear and quadratic filter coefficients respectively. It is easy to see that (1) is a nonlinear equation in terms of the beamformed input data. However, it is a linear equation in terms of the unknown filter coefficients (i.e., linear and quadratic Volterra kernels) $h_L(i)$ and $h_Q(j,k)$. Hence, (1) can be rewritten in vector form:

$$\hat{y}(n+1) = Y^T(n)H \quad (2)$$

where past data vector $Y(n)$ is defind at time n as:

$$Y(n) = \left[y(n), y(n-1), y(n-2),..., y(n-m+1), y^2(n), y(n)y(n-1),..., y^2(n-m+1)\right]^T$$

and the filter coefficient vector H is defined as:

$$H = \left[h_L(0), h_L(1), h_L(2),..., h_L(m-1), h_Q(0,0), h_Q(0,1),..., h_Q(m-1,m-1)\right]^T$$

Note that *m* is the system order, *N* is the total number of filter coefficients [3], which is equal to $(m^2+3m)/2$ assuming symmetrical quadratic kernels (i.e., $h_Q(j,k) = h_Q(k,j)$), and superscript ^{T} is the transpose of a vector or a matrix. Similarly, $\hat{y}(n+2), \hat{y}(n+3),..., \hat{y}(n+m)$ can be represented in the form of (2) and expressed in a matrix form. A system of linear equations is formed in order to find filter coefficients as follows:

$$F = GH \quad (3)$$

where the vector *F* and the data matrix *G* are:

$$F = \left[y(n+1), y(n+2),..., y(n+L)\right]^T$$
$$G = \left[Y(n), Y(n+1),..., Y(n+L-1)\right]^T$$

where L is the number of linear equations (observations). Using a segment of the RF data, a system of linear equations are formed and solved for elements of the quadratic kernel. Details of the algorithm to determine the quadratic kernel that provide maximum contrast enhancement have been described in [3-4].

B. Adaptive Second-order Volterra Filering

In time domain adaptive filters, the new filter coefficients $h_{est}(n+1)$ are updated using old filter coefficients $h_{est}(n)$, and the estimation error $e(n+1)$, multiplied by the weighting vector $w(n+1)$, as follows:

$$h_{est}(n+1) = h_{est}(n) + w(n+1)e(n+1) \quad (4)$$

where

$$e(n+1) = y(n+1) - h_{est}^{T}(n)Y(n+1) \quad (5)$$

that is, the difference between the true observed output (or response) at time $n+1$ and the output "predicted" by the Volterra model. In general, the weighting vector $w(n)$ is determined so that $h_{est}(n)$ can converge to the unique optimum filter coefficients which minimize the quadratic cost function. A block diagram of a second-order Volterra filter to estimate an unknown quadratic nonlinear system is shown in Figure 1, in which the linear and quadratic filter coefficients are recursively updated. There are two well-known algorithms in digital signal processing which guarantee the convergence of the filter coefficients: the least-mean-squares (LMS) algorithm and the recursive least-square (RLS) algorithm [6-7].

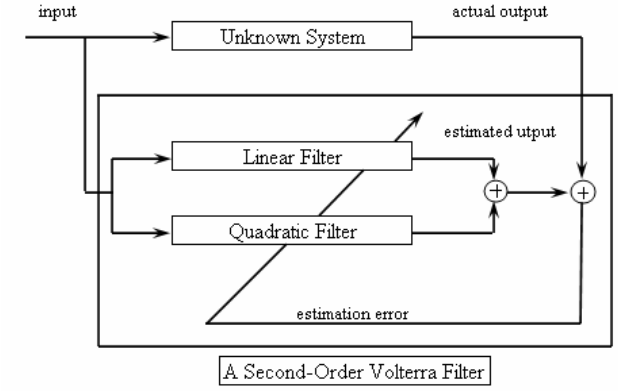

Figure 1 Recursive estimation of an unknown physical system using a second-order Volterra filter, in which a quadratic cost function is minimized and the filter coefficients are recursively estimated using an adaptive filtering algorithm.

In the LMS algorithm, which is an implementation of the stochastic gradient method, the weighting vector is determined by

$$w(n) = 2\mu Y(n) \quad (6)$$

where μ satisfies the convergence condition

$$0 < \mu < \frac{1}{\lambda_{\max}} \quad (7)$$

and $\lambda_{\max}$ is the largest eigenvalue of the matrix GG^{T}. If μ is large while satisfying the convergence condition, the convergence speed of the algorithm is fast, but with large variance (steady-state error). On the other hand, a small μ value reduces the variance, but with slow convergence speed. Therefore, in order to achieve fast convergence and small steady-state error, one might use a "gear shift" that selects relatively large μ initially, and then reduces μ to a small value after the error decreases below a certain level. Since the LMS algorithm can be easily implemented with $O(N)$ computational complexity, it has been widely used in various signal processing applications. However, the LMS algorithm suffers from slow convergence of the filter coefficients, especially when the input is correlated.
In the RLS algorithm, which is an implementation of the stochastic Gauss-Newton method, the weighting vector is determined by

$$w(n) = \left(GG^{T}\right)^{-1} G \quad (8)$$

In fact, the RLS algorithm computes $h_{opt}(n)$ at every instant of time by computing $w(n)$. Hence, the filter coefficients converge quite rapidly, but at the cost of heavy computational complexity, i.e., $O(N^2)$. Thus, various fast RLS (FRLS) algorithms, which are computationally more efficient, have been developed. Since a second-order Volterra filter using the RLS algorithm is more complicated than a linear filter using the RLS algorithm and requires a large number of filter coefficients, the fast implementation of the RLS algorithm for a second-order Volterra filter is desirable in order to reduce the computational complexity, and is often necessary for real-time applications. However, in this paper, the RLS algorithm for a second-order Volterra filter is utilized, instead of the fast RLS algorithm, to obtain the optimum filter coefficients minimizing the cost function to produce images with high sensitivity to nonlinear oscillations (20 - 30 dB below the fundamental) from microbubble ultrasound contrast agents (UCA) while maintaining high levels of noise rejection. The details of the development of the algorithms are beyond the scope of this paper, but may be found in [6-7].

III. MATERIALS AND METHODS

A. Experimental setup

We evaluated the algorithm with RF data acquired from experiments conducted *in vivo* on a juvenile pig. Bolus injections of SonoVue™ (Bracco Research SA, Geneva, Switzerland), an UCA consisting of sulphur hexafluoride gas bubbles coated by a flexible phospholipidic shell, were administered with two different concentrations (0.01 mL/kg and 0.0025 mL/kg).

Three- and four-cycle pulses at 1.56 MHz were transmitted using a convex array probe (CA430E) with mechanical indices (MIs) of 0.158 and 0.152, respectively, to scan a kidney. Technos MPX ultrasound system (ESAOTE S.p.A, Genova, Italy) was modified so that a pair of inverted pulses with the appropriate time delay was subsequently transmitted to produce images

with the PI technique. In addition, in order to remove low frequency components due to tissue motion artifacts and retain harmonic frequency components from UCAs, RF data from PI imaging were filtered using the linear highpass filter with cutoff frequency 2.3 MHz. For each setup, three frames of RF data from the PI technique were collected with 10 s and 15 s delays after the injection of 0.01 mL/kg and 0.0025 mL/kg UCAs, respectively. RF data were acquired with 16-bit resolution at 20-MHz sampling frequency without TGC compensation and saved for off-line processing.

B. Contrast measurements

As a comparison of contrast enhancement between images from different techniques, we compute contrast-to-tissue ratio (CTR) from data in the RF domain before scan converted. CTRs of images can be calculated with echoes from two referenced regions: First, the contrast region inside the kidney (bottom-left part). Second, the tissue region outside the kidney (on the left hand side of the contrast region with the same depth). Both regions are composed of 21 connected A-lines with 7.5-mm axial extent.

IV. RESULTS AND DISCUSSION

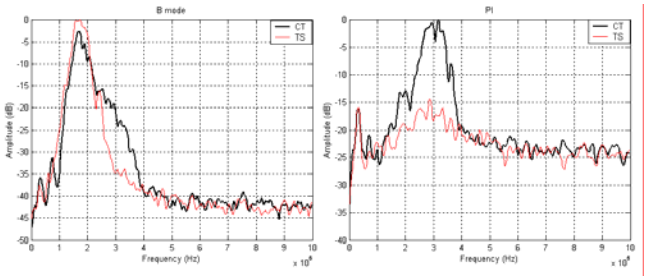

Figure 2 Average spectra from the contrast (darker, black) and tissue (lighter, red) regions of the kidney: Standard B-mode, and PI.

Figure 2 shows the average spectra of typical echoes from the contrast and tissue regions of the kidney described from the standard B-mode and PI data in Section 3. The average spectra are calculated by averaging windowed periodogram of every echo line in regions described in Section 3.2. The echoes from the UCA region exhibit broader bandwidth than those from tissue region

Figure 3 shows images obtained using a standard B-mode image of the kidney after the injection of 0.01 mL/kg UCAs acquired using 3-cycle transmission, PI, second harmonic on PI data (SHPI), quadratic image from twice 2D correlation of 38th singular mode of the B-mode data, and quadratic image from the ASOVF of the B-mode data. Due to differences in dynamic ranges, each image is displayed with its full dynamic range as can be seen from the dB-level scale bars. Due to low microbubble populations in the perfused tissue of the kidney (Standard B-mode image), echogenicity from contrast regions is slightly lower than that from surrounding tissue regions, which agrees with the CTR value (-2.12 dB) whereas the PI image provides CTR 14.36 dB, echogenicity of the contrast region from the PI image appears brighter than that from surrounding tissue regions. Please note that the CTR value for the PI image without SH filtering was only 10.23 dB, i.e. there is a 4.13 dB gain due to the removal of tissue components introduced by motion. It is also worth noting that the SH image on the B-mode data suffers from significant loss in spatial resolution. The quadratic image from twice 2D correlation of 38th singular mode provides CTR 23.13 dB, which shows a contrast enhancement over both standard B-mode, PI and SHPI images.

The quadratic image from the ASOVF of the B-mode data is obtained using the algorithm described in section 2 with the use of a 5.6-mm contrast A-line and a system order 15, provides CTR 34.11 dB, which shows a contrast enhancement over the other four images. We can clearly see not only the kidney's shape and boundary due to UCA echoes but also large vascular structures as it is seen in the PI, SHPI, quadratic from twice 2D correlation of 38th singular mode images too. Also we can see that the kidney's shape and boundary due to UCA echoes are the clearest in the ASOVF image compared with the other four images due to the efficient removal of noise throughout the spectrum while maintaining quadratic data, even below the noise floor.

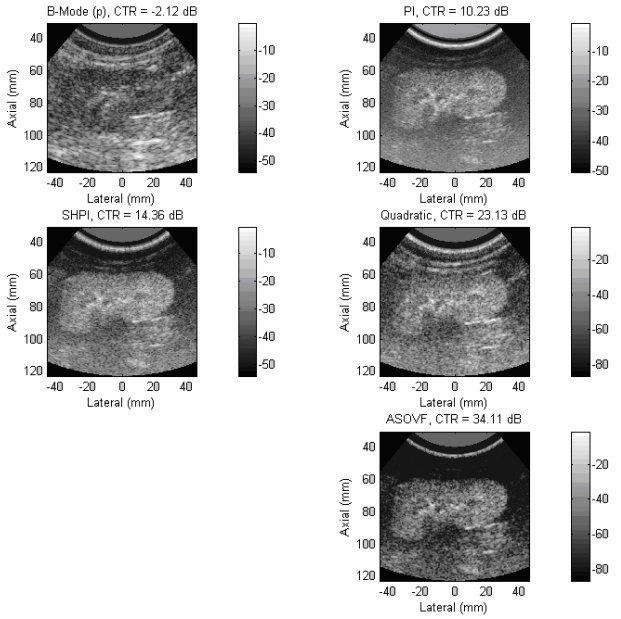

Figure 3 Images of the: Standard B-mode image of the kidney at 10 s after the injection of 0.01 mL/kg, PI, SHPI, quadratic from twice 2D correlation of 38th singular mode of the B-mode data, and quadratic from the ASOVF of the B-mode data.

Figure 4 shows the gray-level histograms produced from the standard B-mode, PI, SHPI, quadratic from twice 2D correlation of 38th singular mode of the B-mode data, and quadratic from the ASOVF of the B-mode data images. In each case, the histogram from the UCA region is plotted with light solid line (red), while the histogram from tissue is plotted with darker solid line (black). One can see the degree of overlap between the histograms is highest for the standard B-mode image, whereas it is the lowest for the ASOVF image.

V. CONCLUSION

We have proposed the new algorithm of post-beamforming adaptive second order Volterra filter (ASOVF) for deriving the quadratic kernels which give the highest CTRs, efficiently remove noise throughout the spectrum, maintaining quadratic data, even below the noise floor, and extract quadratic components from UCA nonlinear echoes with single transmission. Compared with the PI image processed from the same RF data, the quadratic images show comparable performance in terms of both contrast and spatial resolution. The results shown in this paper indicate clearly that ASOVF imaging is far superior to either PI or quadratic imaging. In addition, compared to PI imaging, the Volterra filter approach does not require multiple transmissions for acquiring one image line. Therefore, this approach preserves the frame rate of the original B-mode system, an important advantage of ultrasound imaging over other medical imaging modalities.

REFERENCES

1. J. Ophir and K. J. Parker, “Contrast agent in diagnostic ultrasound,” *Ultrasound in Med. & Biol.*, vol. 15, no. 4, pp. 319-333, Nov. 1989.
2. D. H. Simpson, C. T. Chin, and P. N. Burns, “Pulse inversion Doppler: A new method for detecting nonlinear echoes from microbubble contrast agent,” *IEEE Trans. Ultrason., Ferroelect., Freq. Contr.*, vol. 46, no. 2, pp. 372-382, Mar. 1999.
3. P. Phukpattaranont and E. S. Ebbini, “Post-beamforming second-order Volterra filter for nonlinear pulse-echo ultrasonic imaging,” *IEEE Trans. Ultrason., Ferroelect., Freg. Contr.*, vol. 50, no. 8, pp. 987-1001, Aug. 2003.
4. P. Phukpattaranont, M. F. Al-Mistarihi and E. S. Ebbini, ‘Post-beamforming Volterra filters for contrast-assisted ultrasonic imaging: In-vivo results,” in *Proc. IEEE Ultrason. Symp*., 2003.
5. G. H. Golib and C. F. Van Loan, "Matrix Computations," Johns Hopkins University Press, Baltimore, MD, 2nd edition, 1989.
6. B. Widrow and S. D. Steams, "Adaptive Signal Processing," Englewood Cliffs, NJ: Prentice-Hall, 1985.
7. L. Ljung and T. Söderström, "Theory and Practice of Recursive Identification," Cambridge, MA: M.I.T. Press, 1983.

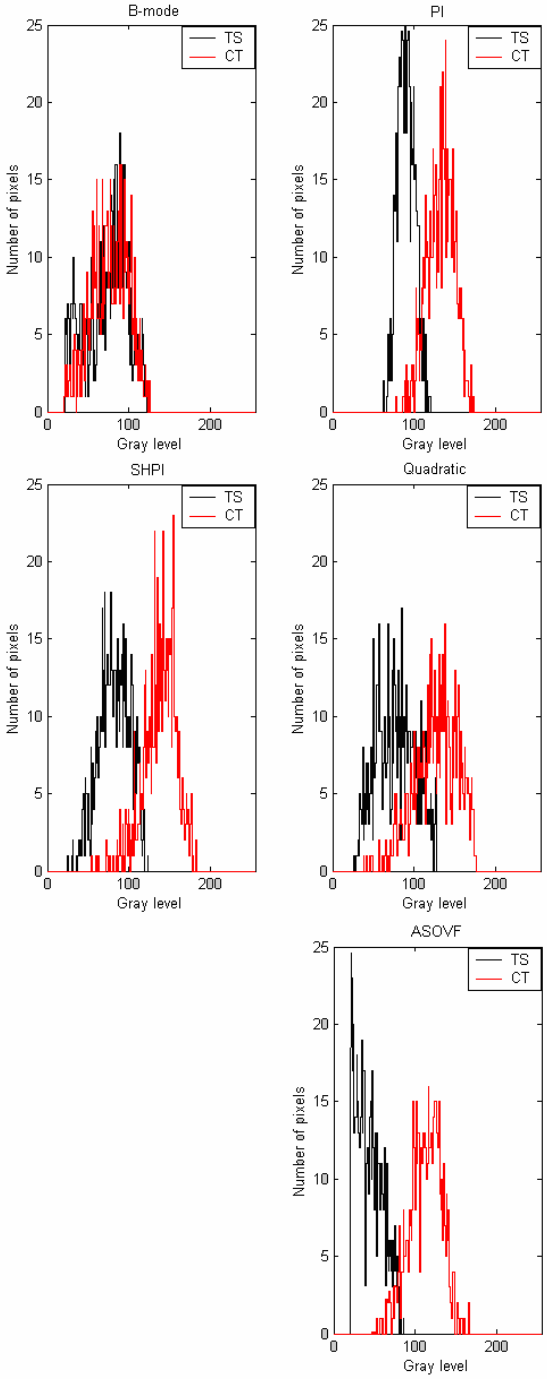

Figure 4 Gray-level histograms produced from images shown in Figure 1. Histograms are produced from the contrast region (lighter, red) and the tissue region (darker, black).